Instruments and Experimental Techniques, Vol. 45, No. 1, 2002, pp. 78–86. Translated from Pribory i Tekhnika Eksperimenta, No. 1, 2002, pp. 87–95.

ELECTRONICS AND RADIO ENGINEERING

A Fast Tunable Detector of Submillimeter Waves on Cyclotron Resonance in an InSb Crystal

G. D. Bogomolov, V. V. Zav'yalov, E. A. Zotova, and E. Yu. Shamparov

Kapitsa Institute for Physical Problems, Russian Academy of Sciences, ul. Kosygina 2, Moscow, 117334 Russia

Received June 25, 2001

Abstract—The design of a detector based on a liquid-helium-cooled *n*-InSb crystal is described, and its performance characteristics are presented. The detector reception band is tunable between 80 and 250 μm (3.75–1.2 THz). The circuit diagrams of its electronic devices (e.g., a wide-band amplifier) are presented, and their operation is described. The detection ability of the detector is 10^{12} cm $Hz^{1/2}$/W at 2 THz.

Sensitive and convenient-to-operate detectors are an important tool in mastering the submillimeter wavelength region ($\simeq 0.03 < \lambda < 1$ mm). At present, in connection with the development of tunable submillimeter free electron lasers (FELs) [1–3], increased requirements of the response speed are additionally imposed on the detectors, which are necessary for detecting pulses of the microsecond duration typical of FEL [1, 2].

Among semiconductor radiation detectors of submillimeter waves, a detector based on the cyclotron-resonance absorption in InSb cooled down to the liquid-helium temperatures can be distinguished [4]. In this crystal, the responsivity to radiation appreciably rises near the cyclotron resonance, making it possible to tune the detector frequency with the use of an external magnetic field, selecting radiation spectrum regions without an additional filtration [5]. The relaxation time of the InSb resistance is rather small (<0.1 μs [6]), and this crystal is suitable for the detection of the envelope of a FEL radiation macropulse [1, 2].

The narrow-band detection of the radiation in the operating wavelength range requires that the InSb crystal must be in an tunable homogeneous magnetic field with a strength of 0.6–1.8 T [7]. Ordinary electromagnets (or solenoids) with such fields have large dimensions and consume high currents. The electromagnet we developed for the detector is a compact superconducting iron-core electromagnet with a magnetic circuit of magnetically soft steel Ст. 3.

Figure 1 shows the design of the electromagnet. It consists of the upper *2* and lower *8* poles, yoke *3*, and a coil *4* (800 turns of a solid copper-plated and varnished NbTi wire with a total diameter of 0.32 mm and a diameter of the superconducting NbTi core of 0.25 mm). A cone with polished walls for guiding the detected radiation to the crystal is cut out in the upper pole along its axis. The angle between the cone's generatrix and axis is 7°. A brass insert *5* with an integrating chamber (its polished walls ensure specular reflection) is placed between the electromagnet's poles. An InSb crystal *7* with dimensions of $3 \times 3 \times 0.8$ mm is glued to the lower pole through a thin quartz plate. The concentration of Sn and Ge impurities in the crystal is 5×10^{13} cm^{-3} (according to the certificate). The lower pole has a

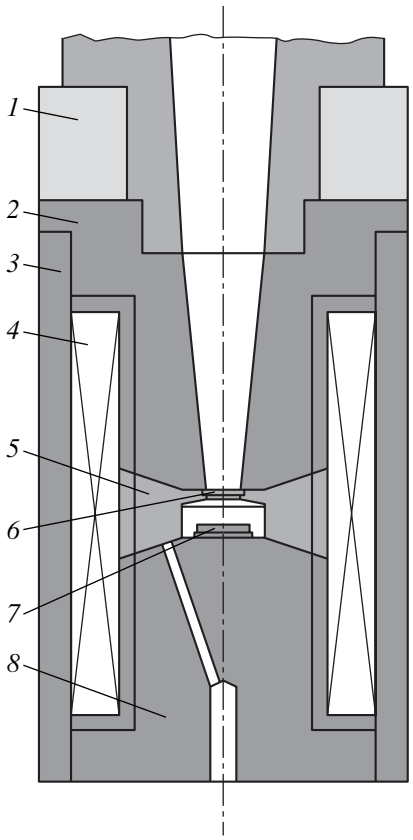

Fig. 1. Schematic drawing (sectional view) of the electromagnet: (*1*) thermal switch; (*2*) upper pole; (*3*) yoke; (*4*) coil; (*5*) brass insert with the integrating chamber; (*6*) cooled window; (*7*) InSb crystal; and (*8*) lower pole.

0020-4412/02/4501-0078$27.00

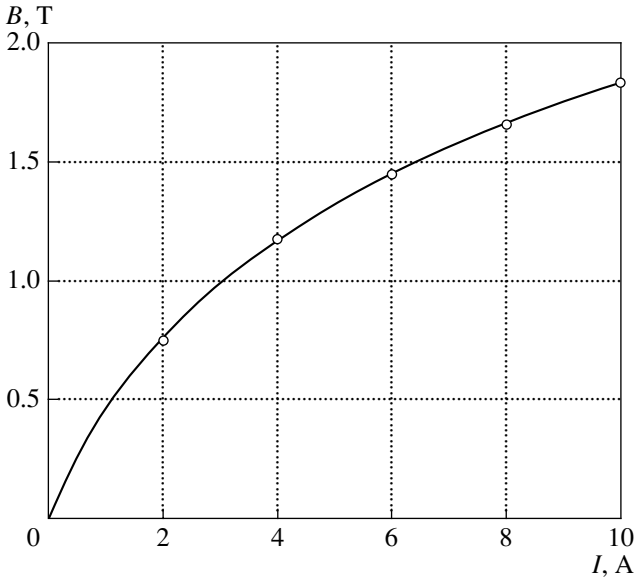

Fig. 2. Magnetic field in the gap of the electromagnet produced by the coil current.

small hole for the connection of measuring wires to the crystal.

By using a program for the calculation of two-dimensional magnetic fields, the shape of the poles and the gap between them were selected so as to obtain the required magnetic field of sufficiently high uniformity at the crystal location at a comparatively small (below 10 A) coil current. According to the calculations, the nonuniformity of the magnetic field $\Delta B/B$ at the crystal location was $\leq 2\%$ at fields of 0.6–1.8 T and the inductance of the electromagnet (at a current of 8 A) was 24 mH.

The magnetic field of the electromagnet cooled by liquid helium was preliminarily measured by a Hall sensor, which was glued to the pole *8* instead of the InSb crystal. The dependence of the field on the current in the coil shown in Fig. 2 is in good agreement with calculations. An additional Hall sensor, which is glued to the lower pole in a small depression near the hole for leading out the measuring wires, is used for magnetic field measurements during the detector operation. The readings of this sensor are calibrated by the current of the electromagnet.

The small size of the electromagnet made it possible to construct the detector in the form of an insert in a domestic helium Dewar vessel (25 l) with a throat 24 mm in diameter. Thus, as compared to the use of a special dewar for the detector, the operation of the instrument is significantly simplified, the time necessary for its cooling and warming is shortened, and the liquid-helium consumption decreases. One filling of the dewar ensures the operation of the detector for at least two weeks.

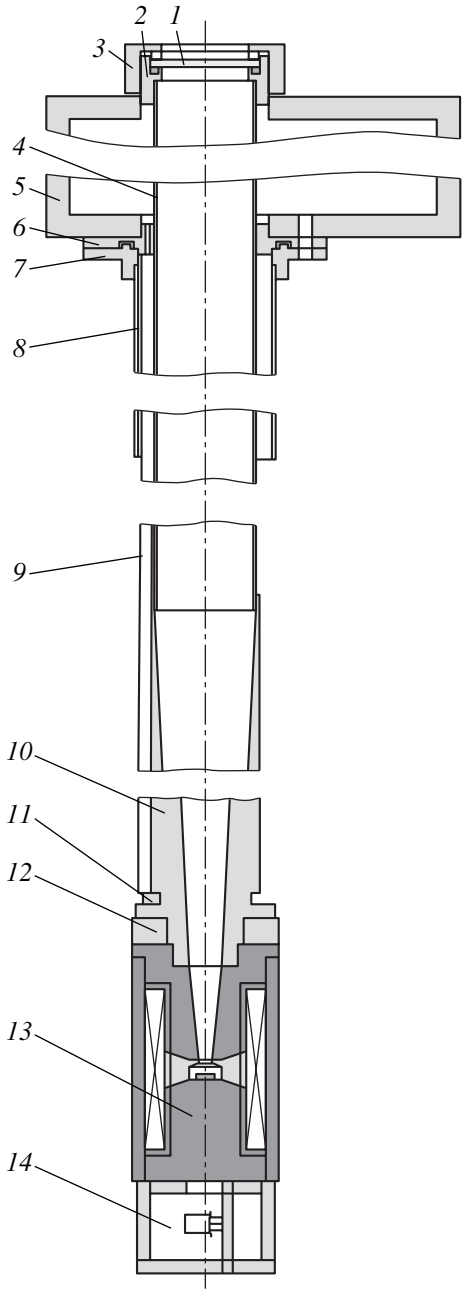

Fig. 3. Schematic diagram of the insert: (*1*) entrance vacuum window (1-mm polyethylene and 0.25-mm black polyethylene); (*2*) flange; (*3*) brass nut tightening the vacuum window; (*4*) waveguide (stainless steel); (*5*) case (Al); (*6*) brass flange connecting the waveguide, case, and the outer tube; (*7*) coupling flange (brass); (*8*) outer tube (stainless steel); (*9*) two tubes for connecting wires (stainless tubes); (*10*) light-collecting cone (brass); (*11*) temperature sensor; (*12*) thermal switch; (*13*) electromagnet; and (*14*) cooled preamplifier.

Figure 3 shows a schematic drawing of the insert. Two coaxial thin-wall (0.3 mm) stainless-steel tubes form the mechanical base of the insert. The upper part of the outer tube *8* (22 mm in diameter) is hermetically soldered into the brass flange *7*. The size of the tube is

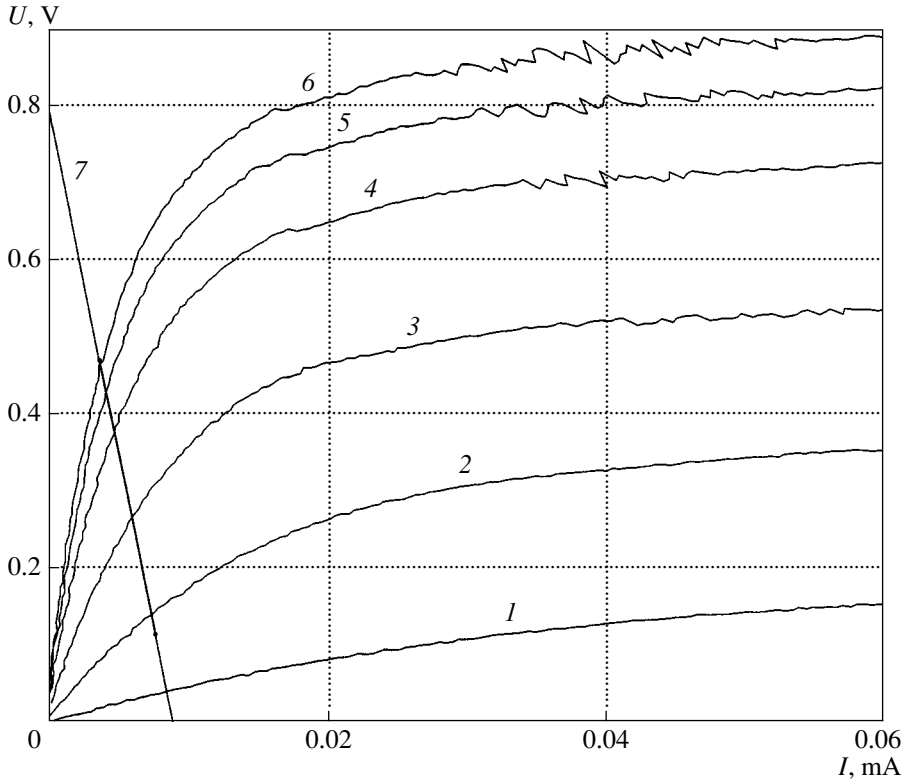

Fig. 4. Current–voltage characteristics of the InSb crystal in various magnetic fields: (*1*) $B = 0$; (*2*) 0.75; (*3*) 1.16; (*4*) 1.45; (*5*) 1.66; and (*6*) 1.83 T; (*7*) dc power supply mode of the crystal in the detector circuit with a selected region corresponding to the detector operating range.

such that, by using an O-ring and a tightening nut, a vacuum-tight joint with the throat of the portable helium Dewar flask is formed, making it possible to control the depth of immersion of the cooled part of the insert into liquid helium. The tube length is such that, for the maximum immersion of the insert, the lower end of the tube does not reach the liquid-helium level in the filled Dewar flask.

The inner tube *4* (16 mm in diameter) with a mirror polish of the inside surface serves as a superdimensional waveguide along which the radiation is guided to the detecting crystal. The radiation is injected through a round flange *2* (at the upper end of the inner tube), which holds a two-layer entrance window *3* (1-mm-thick polyethylene and 0.25-mm-thick black polyethylene) hermetically pressed by a nut *3*. The window intercepts the radiations with wavelengths $\lambda < 25$ μm. A brass cone *10* (the angle between the cone generatrix and axis is 4°) with the polished inside surface is soldered to the lower part of the inner tube. An electromagnet *13* is attached to the brass cone from below. A thermal switch *12* and a carbon resistor *11* (a temperature sensor) are located in two depressions on the outside surface of the cone *10*. The lower end of this cone is smoothly internally jointed to the upper end of the second polished cone cut in the upper pole of the electromagnet (Fig. 1). Both cones form the reception directional diagram with a design angle of 12°. The measured reception pattern coincides with the calculated one rather well.

Passing through the second cone, the radiation enters the integrating chamber, which is intended for increasing the crystal illumination and improving the uniformity of its illuminance over the area. A hole 2 mm in diameter covered by a 1-mm-thick single-crystal quartz disk (*6* in Fig. 1) is the entrance window of the integrating chamber. The pair of the cold quartz and black-polyethylene windows almost intercepts the radiations with $\lambda < 60$ μm [8]. At longer wavelengths, the absorption in the quartz single crystal sharply falls. According to estimates, the part of the radiation reflected from the integrating chamber with the crystal changes from 0.25 (at larger wavelengths) to 0.6 (at $\lambda =$ 80 μm) in the operating wavelength range.

Thin copper wires transmitting signals and feeding the supply voltage run into the Dewar flask through two stainless-steel tubes *9* 3 mm in diameter with 0.1-mm-thick walls. These tubes are soldered to the exterior surface of the inner tube and brass cone and, passing through the gap between the inner and outer supporting tubes, they run to the brass flange *6* hermetically soldered over the inner tube. The wires run outside through two holes in this flange. These holes are filled with picein in order to ensure a vacuum-tight seal, and

an elastic melting glue was deposited on the picein and wires for their mechanical protection. A flange *7*, to which the outer tube is soldered, is attached to the flange *6* from below via a vacuum-tight connector. An aluminum case *5* with dimensions of $140 \times 85 \times 45$ mm containing electronic circuits of the detector and power-supplying battery is fastened to the flange *6* from above. The connectors and elements for controlling the electronic circuits are mounted on the case's surface. The inner stainless-steel tube runs through the case *5* up to its upper surface, on which the entrance vacuum-tight window *1* is fastened to the tube.

The resistance of InSb crystals strongly depends on the magnetic field induction. If an external current source is used to supply the electromagnet, then the noise current component appreciably reduces the detection ability of the detector. Therefore, measurements with the detector are carried out in the persistent mode of the superconducting coil of the electromagnet. The current is injected to the electromagnet and outputted from it by using a thermal switch (*1* in Fig. 1) in which a segment of a NbTi wire changes to the normal state. In order to obtain a superconducting contact in the thermal switch, the ends of the wires led out from the electromagnet were skinned, the copper layer was stripped by etching, and the wires were then welded together by an electric arc. This contact is placed inside a heater (a thin constantan wire with a resistance of 75 Ω). The heater is attached to the body slightly above the electromagnet and is thermally insulated from liquid helium and the insert body by a thin foam polyethylene.

In order to protect the thermal switch from destruction upon transition from the superconducting state to the normal state, it is shunted by a copper wire 5 cm long and 0.3 mm in diameter. The current from an external source is supplied through two varnished copper wires 0.5 mm in diameter to the electromagnet coil, thermal switch, and the shunt connected in parallel. When the heat is switched off, the thermal switch shunts the superconducting winding of the electromagnet. When 5 V (the heating power is 0.33 W) is fed to the heater, the switch changes from the superconducting state to the normal state, and a current from the external source can be inputted into the electromagnet. The time constant of current changes in the electromagnet is ~2 min at the open thermal switch. As a preset current in the electromagnet is reached, the heater is switched off, and the current source can be switched off 5 s later. During the operation of the electromagnet in the short-circuit mode, no perceptible changes in the magnetic field were detected.

Measurements have shown that, in the short-circuit electromagnet mode, the noise component of the detector signal decreases by a factor of 20 as compared to the operation with the electromagnet powered by a П138 stable dc source (I = 4 A).

The detector characteristics substantially depend on the dc current supply regime of the crystal. The regime

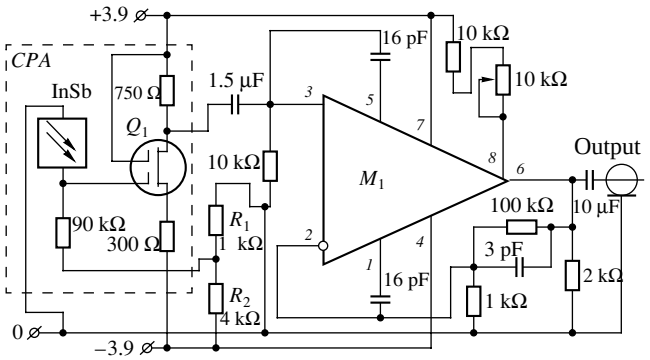

Fig. 5. Amplifier of the signal picked off the InSb crystal: (*CPA*) cooled preamplifier; (M_1) КР1407УД1; and (Q_1) КП350А.

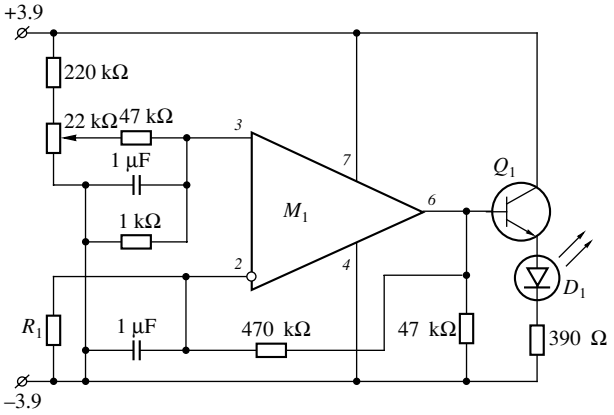

Fig. 6. Temperature sensor: (M_1) LT1077CN8; (Q_1) KT3130E; (D_1) АЛ307АМ; and (R_1) thermoresistor.

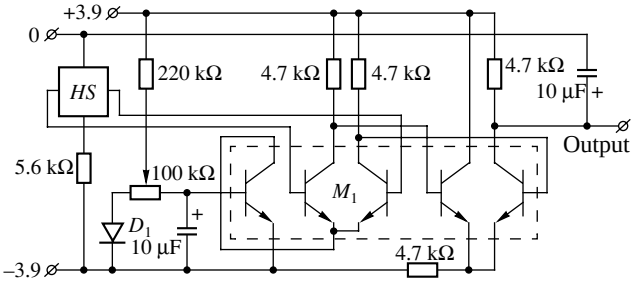

Fig. 7. Amplifier of the signal picked off the Hall sensor: (*HS*) Hall sensor; (M_1) КР198НТ1А; and (D_1) КД514А.

was selected by measuring the crystal current–voltage characteristics (CVCs) at various magnetic field values and room-temperature background radiation incident from the open detector entrance window.

The measurement results are shown in Fig. 4. Local irregularities with sharp changes in the derivative are observed in the CVCs (they are most pronounced in curves *4*–*6*). They are most probably caused by an impact activation of carriers from deep impurity levels

accompanied by breakdown phenomena typical of semiconductors in a cooled state (see, e.g., [5]). When the detector is frequency-tuned by varying the magnetic field, the working point of the crystal (in the current–voltage coordinates) moves along the load characteristic (a straight line) that is determined by the supply voltage and value of the resistor connected in series to the crystal. Experiments have shown that, if the load characteristic passes through the region with irregularities in the CVCs, then sharp nonlinearities appear during the radiation detection and the noise signal component rises even up to the initiation of self-oscillations. The initial region of the CVCs (before the inflexion points in the curves), where such irregularities are absent, is suitable for operation.

A bolometric calculation performed according to a conventional technique [4] yielded the maximum volt–watt responsivity dU/dW of the crystal in the same region.

The resistance of the InSb crystal in the magnetic field is rather high (up to ~150 kΩ). In order to exclude the capacitance of signal wires and, thus, raise the speed of response and improve the interference immunity and noise characteristics of the detector, the signal picked off the InSb crystal is amplified by a cooled preamplifier on a КП350А field-effect (FE) transistor located near the detecting crystal in a small case *14* (Fig. 3), which is attached to the electromagnet from below.

The circuit diagram of the preamplifier is shown in Fig. 5. The circuit was designed by using the CVCs of the InSb crystal (Fig. 4) and the amplification and frequency characteristics of the FE transistor (immersed into liquid helium) measured independently. The circuit is designed so [9] that the operating conditions of the crystal and FE transistor are close to the optimal conditions in the operating wavelength range and the upper frequency of the output signal is ~1 MHz. The final values of the resistors (R_1 = 4 kΩ, and R_2 = 1 kΩ) were selected experimentally by the maximum signal-to-noise ratio at the detector output at the center of the operating wavelength range. For this purpose, the magnetic field was set at a level of 1.3 T, an H_2O laser served as a radiation source, an external supply voltage was fed to the input of the voltage divider formed by the resistors R_1 and R_2, and the dependences of the detector signal and integral noise at the detector output on this voltage were measured. The voltage gain of the preamplifier depends on the resistance of the receiving crystal and changes from 1.6 in the absence of the magnetic field to 0.8 at B = 1.8 T. The upper frequency of the preamplifier decreases with the InSb crystal resistance: from 1.5 MHz (B = 0) to 0.5 MHz (B = 1.8 T). The preamplifier signal is outputted to the outside and is additionally amplified by a factor of 100 by a low-noise amplifier with a passband of 10 Hz–2 MHz based on an КР1407УД1 microcircuit [10].

All electronic circuits of the detector are supplied by a battery of six Ni–Cd accumulators with a low output resistance (~1 Ω each) and a capacity of 0.8 A h. In this case, almost all supply-line interferences and noises, as well as noises produced by other devices are excluded. This is especially significant when using the detector for detecting a pulse FEL radiation. The circuits are powered by a bipolar voltage of ±3.9 V. In order to exclude a contact noise, the connecting wires are soldered to the terminals of the accumulators. When it becomes necessary, the accumulators are charged from a separate source of a stable 80-mA current with a circuit for protecting the battery from voltage overloading upon its complete charge.

Two additional amplifiers (their circuit diagrams are shown in Figs. 6 and 7) are used to monitor the detector operation. The first one amplifies the signal from a carbon sensor measuring the temperature of the cooled detector part. The amplifier is loaded with a visual temperature indicator (a light-emitting diode, LED) located on the case *5* (Fig. 3). The circuit is tuned so that the LED extinguishes as soon as the detector is cooled down to 4.2 K. Such a threshold regime of the detector operation is sufficient for determining the helium level in the Dewar vessel upon immersion of the insert into it and during a long-term operation with the detector. Note that, in the second case, the temperature control is necessary in order to prevent the superconducting coil from destruction in the persistent mode due to the transition into the normal state.

A signal from the Hall sensor measuring the field inside the electromagnet and, thus, the current in the coil (see Fig. 2) during the detector operation is fed to the input of the second amplifier. A dc voltage from the Hall sensor is amplified by a factor of 2000, and a differential signal is transformed into a unipolar signal, significantly simplifying the recording.

The volt–watt and spectral sensitivities of the detector were measured with a light chopper modulating the incoming radiation with a frequency of 200 Hz.

In the first experimental run, in order to carry out the absolute measurements of the detector characteristics to an accuracy acceptable for practice, instead of sources commonly used to imitate a blackbody, it was sufficient to utilize the thermal radiation passing through the detector entrance window from the room. This radiation can be considered sufficiently black, because almost all the surfaces in the room from which the radiation may fall within the detector field of view and the air have high absorption coefficients in the measured wavelength range. Note that during measurements lasting several minutes, the temperature in the room measured by an ordinary thermometer remained constant. Experiments have shown that a spurious illumination of the detector by scattered short-wavelength radiation (from electric sources or window) had almost no effect on the signal when operating with the light chopper. This is determined, on the one hand, by a sig-

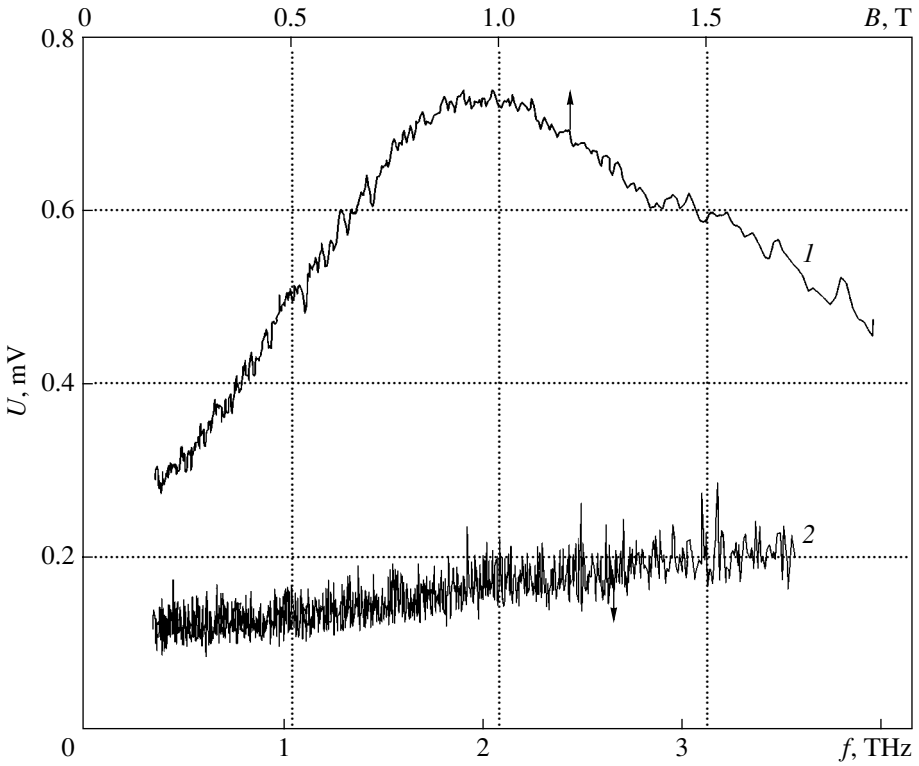

Fig. 8. (*1*) Detector response to the thermal radiation with T = 292 K and (*2*) integral noise at the detector output.

nificantly lower responsivity of the InSb crystal to the radiation beyond its cyclotron absorption band and, on the other hand, confirms the efficiency of the spectral filtration in the detector optical path.

The light chopper was a flat aluminum disk with slits; its polished surface facing the detector entrance window ensured a specular reflection. The chopper plane was perpendicular to the optical axis of the detector and was set at a minimum possible distance (2 mm) from the entrance window.

When the detector entrance window is closed by a specular blade of the light chopper, the crystal is irradiated by the thermal radiation (including that reflected back by the chopper blade) from the specular surface of the optical path, a greater part of which has a temperature much lower than room temperature, and from the entrance polyethylene window having room temperature and being almost transparent in the operating wavelength range. The signal produced by this radiation is at least an order of magnitude weaker than the signal from the thermal radiation from the room at the open slit of the chopper. When the detector with a detection band of up to 1.5 MHz registered the room-temperature radiation, an output meander signal with a signal-to-noise ratio of at least two was observed on the oscilloscope screen.

In order to improve the measurement accuracy when recording the detector output voltage as a function of the magnetic field $U_b(B)$ for the detector illuminated by the room-temperature radiation, a narrow-band reception mode was used. The output signal was fed to the input of a lock-in amplifier (Stanford Research Systems SR830DSP Lock-in Amplifier). A signal from the chopper rotation sensor was fed to its lock input. A signal from the Hall-sensor voltage amplifier arrived at the input of an ADC built in the lock-in amplifier. Both digitized signals were stored in the computer's memory at a frequency of 1 Hz. The current preliminarily injected into the electromagnet was 10 A. The start of the detector signal recording coincided with the turning-on of the thermal-switch heater. When the heater was turned on, the current in the electromagnet coil monotonically decreased. The recording was terminated 5 min later at a current of ~0.5 A. The results of thermal radiation measurements at room temperature (292 K) are presented in Fig. 8.

The second experiment was devoted to measurements of the InSb spectral absorption band, namely, the dependence of the detector amplifier output signal U_l on the magnetic field B for the detector irradiated by a monochromatic line of a water vapor gas-discharge laser [11]. The most detailed measurements were performed at a wavelength of 118 μm lying at the center of the detector spectral range. In these experiments, the light chopper was set rather far from the detector entrance window at an angle of 70° to the laser beam direction in order to exclude the detection of a modulation of a background radiation from the room. The sig-

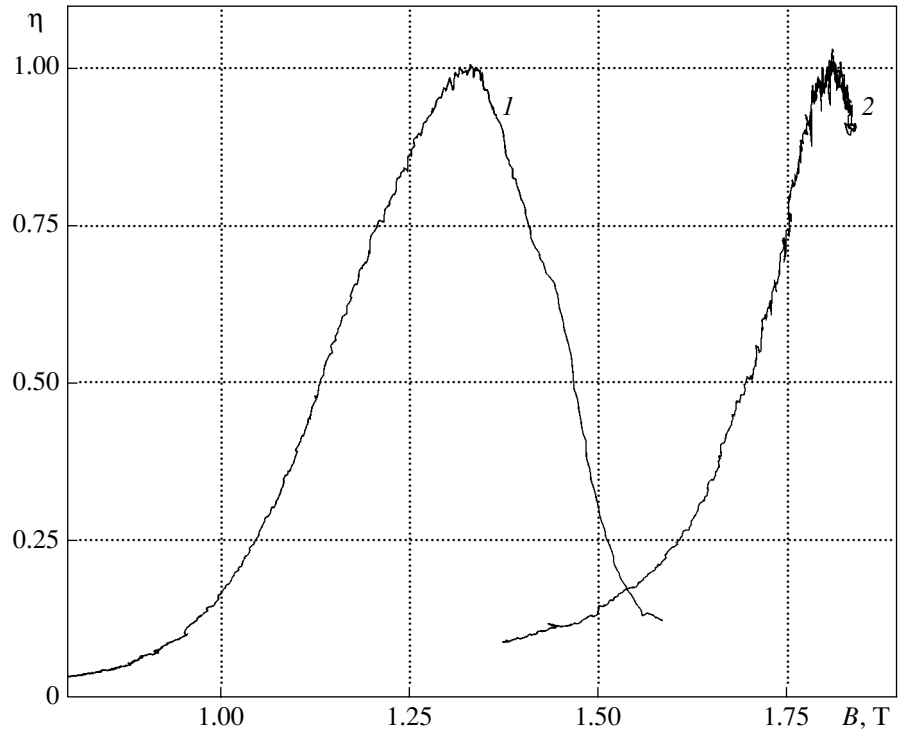

Fig. 9. Curves of resonance absorption of H_2O laser radiation with wavelengths (*1*) 118 and (*2*) 78 μm by the InSb crystal.

nals were recorded according to the same technique that was used in experiments with thermal radiation.

The data processing technique was as follows.

When the external radiation power is sufficiently small, the detector response is proportional to the power W_a absorbed by the InSb crystal.

The InSb crystal placed in a magnetic field B_0 efficiently absorbs radiation at the cyclotron resonance frequency [4, 5, 7]

$$\omega_0 = eB_0/m_* \quad (1)$$

within a frequency band

$$\Delta\omega = -\tau^{-1}, \quad (2)$$

where τ is the time between two successive electron scatterings [12], which is, similar to the frequency band, almost independent of the magnetic field; m_* is the effective mass of charge carriers.

The absorption of radiation with the frequency ω by the crystal placed in the field B_0 can be represented in the form

$$dW_a = \alpha(\omega)\eta(\omega - \omega_0)dW, \quad (3)$$

where dW is the radiation power at the detector input, α is the factor determined by the spectral transparency of the detector optical path and by the reflection of the radiation by the crystal, and η is the efficiency of the resonant absorption of the radiation (at the resonant frequency, $\eta = 1$ can be assumed).

The detector response to the thermal radiation of room temperature at the field B_0 is, according to the Planck formula (for $\hbar\omega << kT$),

$$U_b(B_0) = K(B_0)\beta\int_0^\infty \omega^2\alpha(\omega)\eta(\omega - \omega_0)d\omega, \quad (4)$$

where $K(B_0)$ is the coefficient determined by the dc operating mode of the crystal and

$$\beta = kTA\Omega/4\pi^2c^2. \quad (5)$$

Here, $A = 1.5$ cm^2 is the area of the detector entrance window and $\Omega = 0.01(15°)$ is the measured effective solid angle of view of the detector.

When estimating the thermal radiation power absorbed by the InSb crystal, the actual absorption band was approximated by a rectangular distribution: the absorption efficiency is equal to one between $\omega_0 - \Delta\omega/2$ and $\omega_0 + \Delta\omega/2$ and zero outside of this frequency range. The coefficient $\alpha(\omega)$ is a slowly changing smooth function, and, for $\omega_0 > \Delta\omega/2$, in order to obtain sufficiently accurate estimates, it can be assumed that

$$\alpha(\omega) = \alpha(\omega_0). \quad (6)$$

In this approximation, (4) is reduced to a simple form

$$U_b(B_0) = K(B_0)\beta\omega_0^2\alpha(\omega_0)\Delta\omega. \quad (7)$$

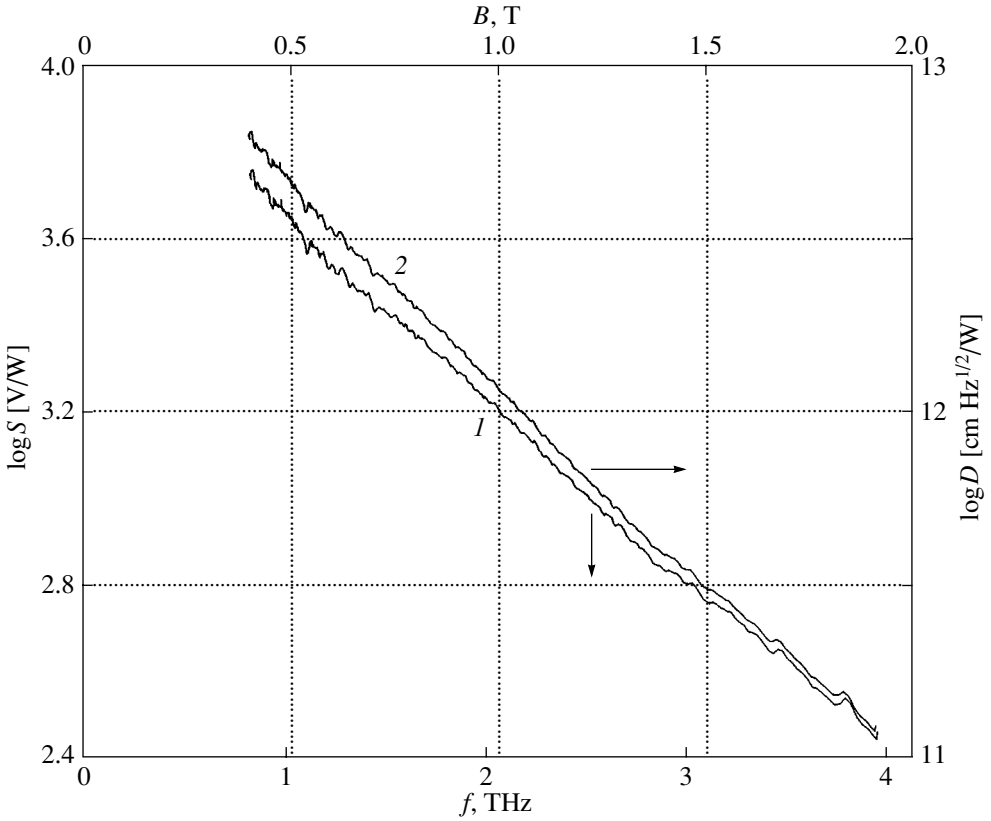

Fig. 10. (*1*) Volt–watt responsivity of the detector as a function of the magnetic field and (*2*) detection ability of the detector.

For the detector illuminated by laser radiation with ω_l and power W_l, the detector response is

$$U_1(B_0) = K(B_0)\alpha(\omega_0)\eta(\omega_0 - \omega_1)W_1. \quad (8)$$

Dividing (8) by (7), in view of (1), we derive

$$\eta(\omega_0 - \omega_1) \sim \frac{U_1(B_0)B_0^2}{U_b(B_0)}, \quad (9)$$

which is the basis for determining the profile of the resonant absorption curve $\eta(B_0)$ (or $\eta(\omega_0)$) from the measurement results described above. Figure 9 shows this curve for the H_2O laser emission line with $\lambda = 118$ μm calibrated at $\eta_{max} = 1$. In this case, the resonance field is $B_0 = 1.30$ T and, consequently, the effective mass of charge carriers in InSb is $m_* = 0.0143m_e$, which is in good agreement with the tabulated data [13]. The half-width of the absorption curve is $\Delta B = 0.35$ T and, thus, the absorption band is $\Delta\omega = 4.4 \times 10^{12}$ rad/s ($\Delta f = 0.7$ THz). The wavelength of the resonance radiation is related to the magnetic field by the expression λ_0, μm = 153/B, T. Figure 9 also shows a record (normalized to unity) of another line with $\lambda = 78$ μm of the H_2O laser lying at the edge of the detector operating range.

As is seen from (7), the volt–watt responsivity of the detector at the resonance frequency

$$S = K(B_0)\alpha(\omega_0) \quad (10)$$

is also calculated from the measurement results (Fig. 10).

The detection ability was determined by measuring the effective integral noise at the detector output as a function of the magnetic field (Fig. 8). For this purpose, the noise from the detector output (the light chopper is absent) was amplified by a broadband amplifier up to a necessary level and was then rectified by a Ge diode. The amplified noise value was fed to the second ADC built in the lock-in amplifier and stored in the computer. The field of the electromagnet was varied and recorded in the same manner that was used in the experiments with thermal radiation. By using the volt–watt responsivity, measured noise voltage, and the known detector speed of response, we calculated its detection ability (see Fig. 11).

Unfortunately, because of the absence of sources of the submillimeter waves of microsecond duration at our disposal, we had no chances to directly measure the response speed of the detector. However, the known response speed of the InSb crystal itself and the amplifier frequency characteristics measured undoubtedly confirm the results obtained.

The detection ability in the submillimeter range of the detector described is somewhat lower than that of the detectors on GaAs epitaxial films and superconducting bolometers, but its response speed is appreciably higher. These characteristics of our detector almost coincide with those of a detector based on pressed

Ge : Ga [2], which was used to detect a FEL macropulse. Note that an additional feature of the InSb detector is its frequency selectivity, which significantly extends its applicability. The spectral characteristic of the detector detection ability is in good agreement with the data from [4].

ACKNOWLEDGMENTS

This work was supported by the Russian Foundation for Basic Research, projects nos. 99-02-16012 and 01-02-17408.

REFERENCES

1. Young Uk Jeong, Byung Cheol Lee, Sung Oh Cho, *et al.*, Abstracts of Papers, *AFEL'99*, KAERI, Taejon, Korea, 1999, p. 96.
2. Ryukuo Kato, Satoshi Kondo, Tetsuya Igo, *et al.*, Abstracts of Papers, *AFEL'99*, KAERI, Taejon, Korea, 1999, p. 107.
3. Vinokurov, N.A., Abstracts of Papers, *AFEL'99*, KAERI, Taejon, Korea, 1999, p. 7.
4. Putley, E., *Phys. Status Solidi*, 1964, no. 6, p. 571; *Dlinnovolnovaya infrakrasnaya spektroskopiya* (Long-wave Infrared Spectroscopy), Moscow: Mir, 1966, p. 177.
5. Seeger, K., *Semiconductor Physics*, Berlin: Springer, 1974. Translated under the title *Fizika poluprovodnikov*, Moscow: Mir, 1977.
6. Yngvesson, S., Abstracts of Papers, *I Swedish–Russian–Finnish School for Young Scientists*, *Chalmersbibliotekets reproservice*, Goteborg, Sweden, 2000, p. 77.
7. Kittel, C., *Introduction to Solid State Physics*, New York: Wiley, 1976, 5th ed. Translated under the title *Vvedenie v fiziku tverdogo tela*, Moscow: Nauka, 1978.
8. Loewenstein, E., Smith, D., and Morgan, R., *Appl. Opt.*, 1973, vol. 12, no. 2, p. 398.
9. Tietze, U. and Schenk, K., *Halbleiter Schaltungstechnic*, Heidelberg: Springer, 1980. Translated under the title *Poluprovodnikovaya skhemotekhnika*, Moscow: Mir, 1982.
10. Novachenko, I.V., Petukhov, V.M., Bludov, I.P., and Yurovskii, A.V., *Mikroskhemy dlya bytovoi radioapparatury: spravochnik* (Microcircuits for Everyday Radio Equipment: A Handbook), Moscow: Radio i Svyaz', 1989.
11. Zav'yalov, V.V. and Bogomolov, G.D., *Prib. Tekh. Eksp.*, 1982, no. 3, p. 174.
12. Landau, L.D. and Lifshits, E.M., *Teoreticheskaya fizika*, vol. 3: *Kvantovaya mekhanika (nerelyativistskaya teoriya)*, Moscow: Fizmatgiz, 1963. Translated under the title *Course of Theoretical Physics*, vol. 3: *Quantum Mechanics: Non-Relativistic Theory*, New York: Pergamon, 1977, 3rd ed.
13. *Fizicheskie velichiny: Spravochnik* (Physical Values: A Handbook), Grigor'ev, I.S. and Meilikhov, E.Z., Eds., Moscow: Energoatomizdat, 1991.